**STLE**

Society of Tribologists
and Lubrication Engineers

# On the Modeling of Elastic Contact between Rough Surfaces

ROBERT L. JACKSON[1] and ITZHAK GREEN[2]

[1]Department of Mechanical Engineering
Auburn University
Auburn, Alabama, USA

[2]Woodruff School of Mechanical Engineering
Georgia Institute of Technology
Atlanta, Georgia, USA

*The contact force and the real contact area between rough surfaces are important in the prediction of friction, wear, adhesion, and electrical and thermal contact resistance. Over the last four decades various mathematical models have been developed. Built on very different assumptions and underlying mathematical frameworks, model agreement or effectiveness has never been thoroughly investigated. This work uses several measured profiles of real surfaces having vastly different roughness characteristics to predict contact areas and forces from various elastic contact models and contrast them to a deterministic fast Fourier transform (FFT)-based contact model. The latter is considered "exact" because surfaces are analyzed as they are measured, accounting for all peaks and valleys without compromise. Though measurement uncertainties and resolution issues prevail, the same surfaces are kept constant (i.e., are identical) for all models considered. Nonetheless, the effect of the data resolution of measured surface profiles will be investigated as well. An exact closed-form solution is offered for the widely used Greenwood and Williamson (GW) model (Greenwood and Williamson, Proceedings of the Royal Society of London A, vol. 295, pp. 300–319), along with an alternative definition of the plasticity index that is based on a multiscale approach. The results reveal that several of the theoretical models show good quantitative and qualitative agreement among themselves, but though most models produce a nominally linear relationship between the real contact area and load, the deterministic model suggests otherwise in some cases. Regardless, all of the said models reduce the complicated surface profiles to only a few key parameters and it is therefore unrealistic to expect them to make precise predictions for all cases.*

## KEY WORDS

## INTRODUCTION

For practicing engineers in industry it is important to have closed-form, easy-to-use equations that can be used to predict the real contact area and relate it to the friction, wear, adhesion, and electrical and thermal contact resistance. The ability to accurately predict real contact area as a function of load for rough surface contact is a difficult task due to the complex nature of real surfaces. Many models have been proposed over the years for the prediction of the real area of contact between rough surfaces. One of the very first of these models is that by Archard *(1)*, who showed that although single asperity contact might result in a nonlinear relation between area and load, by incorporating multiple scales of roughness the relationship becomes linear. Archard *(1)* used a concept where spherical asperities are stacked upon each other, each with a smaller radius of curvature. This stacked-type model had largely been abandoned after the statistics-based Greenwood and Williamson *(2)* (GW) model was published in 1966. Since then, that model did not have a closed-form solution because of the complexity of carrying out the integrals when a Gaussian distribution is used to describe surface roughness.

Later researchers thought that the multiple scales of asperities present on surfaces needed to be considered, so fractal methodologies have been formulated (Majumdar and Bhushan *(3)*; *(4)*; Warren and Krajcinovic *(5)*; Willner *(6)*; Yan and Komvopoulos *(7)*). However, fractal models were also found to have deficiencies. For example, the most notable deficiencies of the Majumdar and Bhushan *(3)* (MB) fractal model are that the contact area is calculated from truncation and that it predicts less plastic deformation with increasing loads. Hence, a few other methods that consider multiple scales of roughness have been proposed (Ciavarella and Demelio *(8)*; Ciavarella, et al. *(9)*; Bora, et al. *(10)*; Jackson and Streator *(11)*; Persson *(12)*).

A handful of these models will be implemented in the current work and compared to a deterministic elastic contact model that uses a fast Fourier transform (FFT) to improve computational efficiency (Stanley and Kato *(13)*). The deterministic model is considered exact because surfaces are analyzed as they are without compromising the details. That is, every single peak is considered in the progression of contact. The surfaces analyzed

Nomenclature

| | | |
|---|---|---|
| $A$ | = | Area of contact between local asperities |
| $A_n$ | = | Nominal contact area |
| $A_r$ | = | Real contact area between rough surfaces |
| $a$ | = | Nondimensional distance between the mean asperity height |
| $B$ | = | Ratio of surface amplitude to wavelength, $\Delta/\lambda$ |
| $C$ | = | Critical yield stress coefficient |
| $D$ | = | Fractal dimension |
| $d$ | = | Separation of mean asperity height |
| $E$ | = | Elastic modulus |
| $E'$ | = | Equivalent elastic modulus $[(1 - v_1^2)/E_1 + (1 - v_2^2)/E_2)]^{-1}$ |
| erfc | = | Complementary error function |
| $F$ | = | Contact force |
| $f$ | = | Frequency of sinusoidal surface (reciprocal of wavelength, $1/\lambda$) |
| $G$ | = | Fractal roughness |
| $g_n$ | = | Fractal geometric parameter |
| $H$ | = | Hardness |
| $h$ | = | Separation between the mean surface height |
| $I$ | = | Modified Bessel function of first kind |
| $I_{ea}$ | = | Elastic contact area integral for the GW model |
| $I_{ep}$ | = | Elastic pressure integral for the GW model |
| $K$ | = | Modified Bessel function of second kind and hardness factor |
| $\bar{m}$ | = | RMS surface slope |
| $m_n$ | = | $n$th Spectral moment of the surface |
| $N$ | = | Number of surface data points |
| $P_r$ | = | Real contact pressure (average pressure over $A_r$) |
| $p^*$ | = | Pressure amplitude or average pressure required to obtain complete contact |

| | | |
|---|---|---|
| $\bar{p}$ | = | Average pressure over the nominal area of contact of a local asperity |
| $p_e$ | = | Average pressure over the nominal area of contact between rough surfaces |
| $R$ | = | Radius of hemispherical asperity |
| $S_y$ | = | Yield strength |
| $x$ | = | Lateral location on surface |
| $y_s$ | = | Distance between the mean asperity height and the mean surface height |
| $z$ | = | Height of asperity measured from the mean of asperity heights |
| $\alpha$ | = | Nondimensional statistical variable |
| $\beta$ | = | Nondimensional product of the statistical values, $\eta R \sigma$ |
| $\Gamma$ | = | Gamma function |
| $\Delta$ | = | Amplitude of sinusoidal surface |
| $\eta$ | = | Area density of asperities |
| $\theta$ | = | Nondimensional statistical variable |
| $\lambda$ | = | Wavelength of sinusoidal surface (reciprocal of frequency, $1/f$) |
| $v$ | = | Poisson's ratio |
| $\sigma$ | = | Standard deviation of surface heights |
| $\sigma_s$ | = | Standard deviation of asperity heights |
| $\varphi$ | = | Distribution function of asperity heights |
| $\psi$ | = | Plasticity index |
| $\psi_m$ | = | Alternative multiscale plasticity index |
| $\omega$ | = | Interference between hemisphere and surface |

**Subscripts and Superscripts**

| | | |
|---|---|---|
| $c$ | = | Critical value at onset of plastic deformation |
| $max$ | = | Maximum value over all scales |
| $*$ | = | Normalized by $\sigma$ |

here are taken from actual measurements and used throughout. The purpose is to examine model effectiveness and evaluate their common agreement to lend confidence in their results. Other researchers have also made comparisons but not always using real surface data and not considering as many models as are in the current work. McCool *(14)* made an early comparison between the GW (Greenwood and Williamson *(2)*) model and the Bush, et al. *(15)* model and concluded that the GW model is the more effective of the two. Persson, et al. *(16)* compared their elastic diffusion–based contact model to numerical predictions. A comparison between various statistical models was made by Jackson and Green *(17)*. Additionally, a comparison between fractal and statistical models was made by Kogut and Jackson *(18)*. Hyun, et al. *(19)* also performed an elastic finite element method (FEM) model of rough surface contact between artificially generated self-affine surfaces and made comparisons to Persson *(12)* and Bush, et al. *(15)* that showed agreement within an order of magnitude, with Persson's model performing the best.

Similar to the ubiquitous GW model (Greenwood and Williamson *(2)*), the current work focuses only on the elastic regime of contact. As presented in the GW model, the range of model validity (caused by the likely occurrence of plastic deformation under heavy loads) is delegated to a plasticity index, which has become a popular way to determine the relative amount of plastic deformation occurring in a rough surface contact. The GW plasticity index is based on a single scale of the statistical parameters. The main objective of the current work is to make a comparison of several elastic rough surface contact models (in addition to GW) using measured data of real surfaces and compare the results to an FFT-based deterministic model. The current work complements the GW model by offering for the first time an exact closed-form solution for that model when a Gaussian distribution is used, along with an alternative method to define a plasticity index that is based on a multiscale approach to rough surface contact (see Appendix). With this in mind, that is, that the analysis is limited to purely elastic surfaces, the range of deformation is rather a moot point, and excluding the intricacy of plastic deformation allows for a straightforward comparison between the various elastic contact models. Nonetheless, there are some surfaces, such as rubber, that will deform entirely in the elastic regime even at high loads. The intent here is also to evaluate the effects of data resolution on the various models that are built on very different assumptions and underlying mathematical frameworks.

## METHODOLOGY

This section describes the methodology used to make predictions of the real contact area and the contact force using five different contact models as they are applied to the contacting roughness of three real surfaces measured by a laser profilometer. The models are the following:

1. Stanley and Kato's *(13)* FFT deterministic elastic contact model

2. Closed-form solutions to the GW contact model (with a Gaussian distribution)
3. Bush, et al.'s *(15)* statistical contact model
4. Persson's *(12)* diffusion contact model
5. Stacked multiscale model (Jackson *(20)*)

Each of these models is discussed in more detail in the following sections. Nevertheless, for more details (such as complete derivations) the reader is referred to the original papers. The current work will also make comparisons for different surface mesh densities.

## FFT Deterministic Elastic Contact Model

In this section, an existing FFT-based rough surface contact model is summarized and its predictions are verified by comparing results to a known analytical solution. Stanley and Kato *(13)* (SK) presented a simple algorithm to model rough surface contact using an FFT. This method is used here because it provides for a faster computational solution than a conventional FEM model would. The contact pressure is first transformed into the frequency domain. Then the deflection is solved in the frequency domain by multiplying the pressure by an appropriate stiffness matrix and transforming it back using an inverse FFT. The details of the model can be found in Stanley and Kato *(13)*. The work is implemented here in 3D and validated by comparing to a 3D model of elastic sinusoidal contact (Johnson, et al. *(21)*). The asymptotic solutions of 3D sinusoidal contact were found by Johnson, et al. *(21)* (referred to as JGH) and are given as:

- For $\frac{\bar{p}}{p^*}$ approaching 0:

$$(A_{\text{JGH}})_1 = \frac{\pi}{f^2} \left[ \frac{3}{8\pi} \frac{\bar{p}}{p^*} \right]^{2/3} \qquad [1]$$

- For $\frac{\bar{p}}{p^*}$ approaching 1:

$$(A_{\text{JGH}})_2 = \frac{1}{f^2} \left( 1 - \frac{3}{2\pi} \left[ 1 - \frac{\bar{p}}{p^*} \right] \right) \qquad [2]$$

where $p^*$ is the average pressure to cause complete contact between the surfaces and is given by Johnson, et al. *(21)* as:

$$p^* = \sqrt{2}\pi E' \Delta f \qquad [3]$$

and $\bar{p}$ is the average pressure over the nominal area of contact of a local asperity. Then, based on numerical and experimental data provided by JGH and Krithivasan and Jackson *(22)*, an equation is fit to bridge the gap between the solutions of Jackson and Streator *(11)* and Krithivasan and Jackson *(22)*). Hence, it is given as:

- For $\frac{\bar{p}}{p^*} < 0.8$

$$A = (A_{\text{JGH}})_1 \left( 1 - \left[ \frac{\bar{p}}{p^*} \right]^{1.51} \right) + (A_{\text{JGH}})_2 \left( \frac{\bar{p}}{p^*} \right)^{1.04} \qquad [4]$$

- For $\frac{\bar{p}}{p^*} \geq 0.8$

$$A = (A_{\text{JGH}})_2 \qquad [5]$$

A 3D sinusoidal surface is substituted into the Stanley and Kato *(13)* model and the resulting prediction of contact area versus pressure is compared to the above 3D sinusoidal model (see Fig. 1). The two models are in close agreement, which confirms the validity of the FFT model. For comparison with the other models, actual measured surface data are then input into the Stanley and Kato *(13)* model and the contact area is predicted for various loads. The only manipulation of the surface data is
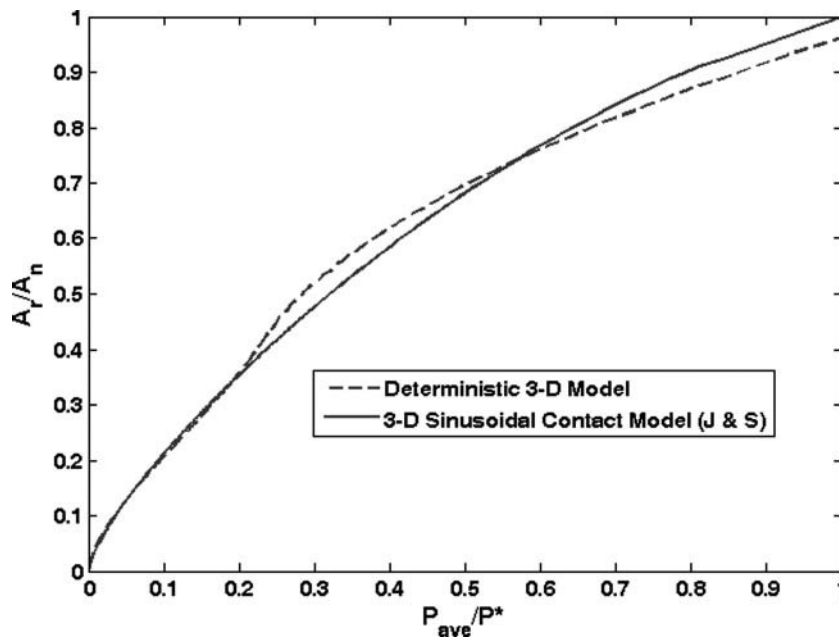


Fig. 1—Comparison of elastic 3D sinusoidal contact and FFT deterministic model predictions.

that they are leveled (the overall tilt is removed) before being entered into the code (the surfaces in contact are nominally flat). The contact area is simply calculated by taking the ratio between the nodes with positive forces and those with zero force (no contact). The real contact pressure is calculated by averaging all of the positive pressures on the surface.

## Closed-Form Solutions to GW Contact Model (with a Gaussian Distribution)

The fundamental GW model (Greenwood and Williamson *(2)*) contains summations (i.e., integrations) to accumulate statistically properties of the rough surfaces for load and real area of contact. Because of the complexity associated with the Gaussian distribution, users of the model have commonly calculated the various integrals numerically. To bypass such cumbersome numerical integrations, the Gaussian distribution has frequently been replaced with simplified exponential distribution functions to allow for closed-form solutions (see the original work by Greenwood and Williamson *(2)*; Etsion and Front *(23)*; Polycarpou and Etsion *(24)*; Hess and Soom *(25), (26)*; and Liu, et al. *(27)*). Then, the GW model laid the foundation for elastic–plastic contact models, one of which is the model by Chang, et al. *(28)* (CEB). Again, the integrals are commonly calculated numerically. A successful attempt was given by Green *(29)*, who provided closed-form solutions to the CEB model. In the elastic range the solution is based on the mean value theorem, whereas in the plastic range the solution is mathematically exact. Because the current work is limited to the elastic deformation only, plasticity is moot. Hence, the solution provided by Green *(29)* cannot be used because of the unlimited range of the elastic deformation. Because the current work focuses on closed-form models, here for the first time, closed-form solutions to the original integrals of the venerable GW model (Greenwood and Williamson *(2)*) are provided; that is, (1) the Gaussian distribution is not compromised (i.e., not simplified nor replaced), (2) the integration results are obtained for the entire deformation range, and the expressions provided are mathematically exact. That is, the solution here makes any approximation of the Gaussian distribution (as mentioned above) or numerical integration unnecessary.

This work adheres to the definitions and nomenclature of CEB (Chang, et al. *(28)*) and Etsion and Front *(23)*, and the reader is referred to these works. Hence, $\beta = \eta R \sigma$, where $\eta$ is the areal density of asperities, $R$ is the asperity radius of curvature, and $\sigma$ is the standard deviation of surface heights. Further, $h^* = h/\sigma$ is the dimensionless mean separation, $\sigma_s^* = \sigma_s/\sigma$ is the dimensionless standard deviation of asperity heights, and $y_s^* = y_s/\sigma$ is the dimensionless distance between the means of asperity and surface heights. Following Green *(29)*, the average elastic contact pressure is $\bar{p} = F/A_n$, where $F$ is the total external force (or load), and $A_n$ is the nominal (or apparent) contact area. The pressure, $\bar{p}$ is further normalized by the equivalent modulus of elasticity. Likewise, the elastic real area of contact, $A_r$, is normalized by the nominal area, $A_n$. Both are given, respectively, by,

$$\frac{\bar{p}}{E'} = \frac{4}{3} \beta \left(\frac{\sigma}{R}\right)^{1/2} I_{ep} \qquad [6a]$$

$$\frac{A_r}{A_n} = \pi \beta I_{ea} \qquad [6b]$$

where

$$I_{ep} = \int_a^\infty (z^* - a)^{3/2} \varphi^*(z^*) \, dz^* \qquad [7a]$$

$$I_{ea} = \int_a^\infty (z^* - a) \varphi^*(z^*) \, dz^* \qquad [7b]$$

The integrals contain a lower bound having the following definition $a = h^* - y_s^*$. The Gaussian distribution is given by

$$\varphi^*(z^*) = \frac{1}{\sqrt{2\pi}} \left(\frac{\sigma}{\sigma_s}\right) \exp\left[-0.5 \left(\frac{\sigma}{\sigma_s}\right)^2 z^{*2}\right] \qquad [8]$$

The integrals of Eqs. [7] are the subject of the discussion above. For conciseness, only the final results of the closed-form solutions are given. Using the definitions $\alpha = a/\sigma_s^*$ and $\theta = \alpha^2/4$ we have

$$I_{ep} = \begin{cases} \sigma_s^* \sqrt{a} e^{-\theta} \left[(1+\alpha^2)K_{1/4}(\theta) - \alpha^2 K_{3/4}(\theta)\right]/(4\sqrt{\pi}) & \text{for } a > 0 \\ \Gamma(5/4)(\sigma_s^*)^{3/2}/(2^{1/4}\sqrt{\pi}) & \text{for } a = 0 \\ (\sigma_s^*/4)\sqrt{-a} e^{-\theta} \sqrt{\tfrac{\pi}{2}} \left[(1+\alpha^2)I_{-1/4}(\theta) \right. \\ \left. + (3+\alpha^2)I_{1/4}(\theta) + \alpha^2(I_{3/4}(\theta) + I_{5/4}(\theta))\right] & \text{for } a < 0 \end{cases} \qquad [9a]$$

$$I_{ea} = \sqrt{\frac{1}{2\pi}} \sigma_s^* e^{-\alpha^2/2} - \frac{a}{2} \text{erfc}\left(\frac{\alpha}{\sqrt{2}}\right) \qquad [9b]$$

where $\Gamma(\cdot)$ is the gamma function; $I(\cdot)$ and $K(\cdot)$ are the modified Bessel functions of the first and second kinds, respectively; and $\text{erfc}(\cdot)$ is the complementary error function. Substitution of Eqs. [9] into Eqs. [6] provides the desired closed-form solution to the GW model (Greenwood and Williamson *(2)*). Interestingly, when an exponential distribution is adopted (instead of a Gaussian distribution), the original GW model suggested that there is a linear relationship between contact area and load, but this solution (Eqs. [6] and [9]) suggests otherwise. The solution given by Eqs. [6] and [9] is used throughout this work and is referred to in the figures as "G&W Gaussian."

Because this is a statistical method, it hinges upon obtaining statistical parameters, $\eta$, $R$, and $\sigma$, described above. To find these parameters, the spectral moments can be employed:

$$m_o = \frac{1}{N} \sum_{n=1}^N (z)_n^2 \qquad [10]$$

$$m_2 = \frac{1}{N} \sum_{n=1}^N \left(\frac{dz}{dx}\right)_n^2 \qquad [11]$$

$$m_4 = \frac{1}{N} \sum_{n=1}^N \left(\frac{d^2 z}{dx^2}\right)_n^2 \qquad [12]$$

where $N$ is the total number of data points on the surface and $z$ is the surface height relative to its mean. The derivatives in Eqs. [11] and [12] are calculated using a centered finite difference scheme. It should be noted that Eqs. [10–12] are for two dimensions. In this work, the 3D data are split into individual 2D rows. Each

row of data is used to calculate $m_2$ and $m_4$. The average value for all the rows is then calculated. Columns of data perpendicular to these rows are also used with no significant change in the predicted values of $m_2$ and $m_4$. The moment $m_0$ is simply the square of the root mean square (RMS) surface height, $\sigma$. The radius of curvature, $R$, and the areal asperity density, $\eta$, are then calculated by using spectral moments (Eqs. [10–12]) and the methods given by McCool (30). Hence,

$$\sigma = \sqrt{m_o} \qquad [13]$$

$$\eta = \left(\frac{m_4}{m_2}\right)\left(\frac{1}{6\pi\sqrt{3}}\right) \qquad [14]$$

$$R = 0.375 \cdot \left(\frac{\pi}{m_4}\right)^{0.5} \qquad [15]$$

### Bush, et al.'s Statistical Contact Model

In this section, the popular model by Bush, et al. (15) (BGT) is summarized. BGT essentially extended the GW model (Greenwood and Williamson (2)) to consider not only a distribution of the surface asperity heights (as was also investigated by Jackson (31) and Onions and Archard (32)) but also a distribution of the asperity curvatures and asperities that do not possess a constant radius of curvature (elliptical). Because this model is supposedly more general, some claim that it is more accurate than the GW model (Hyun, et al. (19)). Interestingly, they found that the real contact pressure is related solely to the elastic properties and the RMS slope of the surface ($\bar{m}$). Note that $\bar{m} = \sqrt{m_2}$ (see Eq. [11]). The equation given by Bush, et al. (15) as an asymptotic solution to their complete model for large surface separations that will used in this work is

$$A_r = \sqrt{\pi}\frac{F}{E'\bar{m}} \qquad [16]$$

This asymptotic solution to the Bush, et al. (15) model also predicts a linear relationship between the contact area and load.

In response to claims that the BGT model (Bush, et al. (15)) is more accurate than the GW model (Greenwood and Williamson (2)), Greenwood formulated a similar but more simplified elliptical model (Greenwood (33)). For typical surfaces, the Greenwood elliptical model finds that the real area of contact is nearly identical to the BGT model.

### Persson's Diffusion Contact Model

The diffusion-based rough surface contact model by Persson (12) is summarized in this section. Because surfaces are structured with successive and perhaps a continuous layering of asperities at various scales, Persson (12) used a diffusion theory to model rough surface contact. Although admittedly Persson's theory is fairly difficult to follow and implement, Hyun, et al. (19) provided a simplified form that is of the same form as the BGT model (Bush, et al. (15)) and Greenwood's elliptical model (Greenwood (33)):

$$A_r = \sqrt{\frac{8}{\pi}}\frac{F}{E'\bar{m}} \qquad [17]$$

However, Carbone and Bottiglione (34) provided a different and more accurate version of Persson's (12) model:

$$\frac{A_r}{A_n} = \mathrm{erf}\left(\frac{F}{A_n E'\bar{m}}\right) \qquad [18]$$

Equation [18] will be used in the current work to consider Persson's (12) model. Interestingly, the models given by Bush, et al. (15); Greenwood (33); and Persson (12) are within an order of magnitude of agreement. Hyun, et al. (19) and Pei, et al. (35) also showed that the models by Bush, et al. (15) and Persson (12) appear to agree fairly well with deterministic finite element models for artificially generated fractal surfaces.

### Stacked Multiscale Model

A recently published stacked multiscale model (Jackson (20)) is summarized in this section. Archard (1) first showed that a linear relationship between the real contact area and load is predicted by using a stacked asperity approach to rough surface contact. However, Archard's (1) model is built upon the concept of stacked asperity scales, each with asperities all with the same radius of curvature, and provides no practical methodology for extracting this information from a measured surface profile. This might be one reason why the Greenwood and Williamson (2) model later gained much more popularity. Much later, Ciavarella and Demelio (8) and Ciavarella, et al. (36) used the Weierstrass surface profile to define the different scales of asperities present on the surface and then implemented Archard's (2) stacked scale model. They found that for a self-affine surface, as described by the Weierstrass–Mandelbrot function, the contact area will be zero with infinite pressures present at each asperity. Jackson and Streator (11) (JS) used a similar methodology except that all the scales are described by the Fourier series extracted from the surface. They found that for some surfaces the area did converge to a finite value (the surfaces were apparently not self-affine). Although it is somewhat a deterministic type model, the JS model also predicted the nearly linear relationship between real contact area and load.

The stacked multiscale model (Jackson (20)) used in this work is a simplified solution of the full multiscale model presented by Jackson and Streator (11). In addition, the new versions (Jackson (20); and Wilson, et al. (37)) employ sinusoidal shaped asperities instead of the popular assumption of using spherical-shaped asperities. The real contact pressure is defined by the pressure required to obtain complete contact at the scale with the largest ratio between amplitude and wavelength [$B_{max} = (\Delta/\lambda)_{max}$] over a spectrum taken of the surface profile. Then the area of contact is given by (Jackson (20)):

$$A_r = \frac{F}{\sqrt{2}\pi E' B_{max}} \qquad [19]$$

This is also analytically derived in Jackson (20). $B_{max}$ is calculated by taking the FFT of each 2D row of the 3D surface and then averaging the results. Columns of data perpendicular to these rows are also used with no significant change in the predicted value of $B_{max}$.
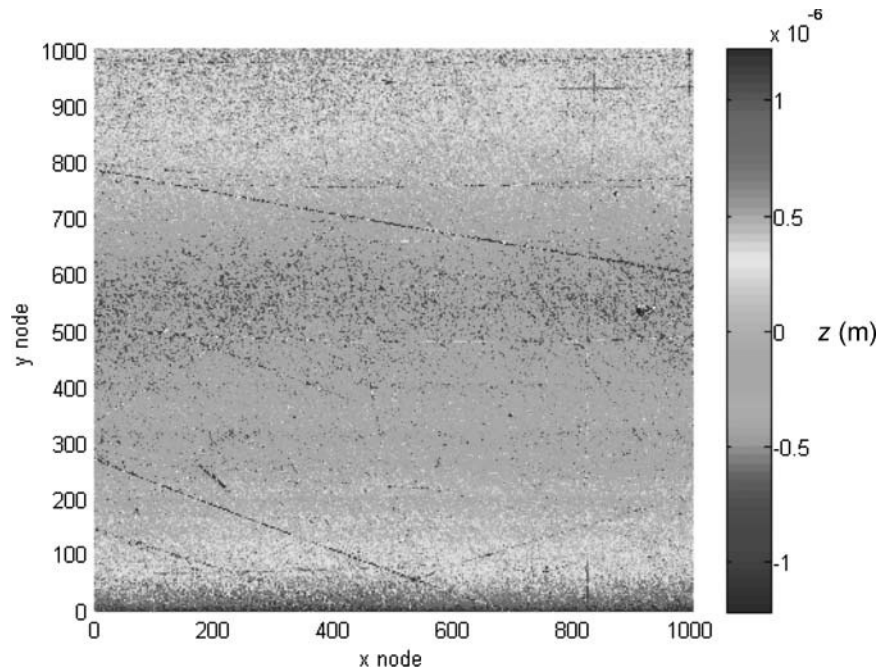
Fig. 2—Measured profile of surface 1.

## Other Models

There are, of course, other contact models available; however, the authors chose those that have gained sufficient practical acceptance (the GW model; Greenwood and Williamson *(2))* and some most recent and relevant models. An attempt was made to also use the fractal-based model by Majumdar and Bhushan *(3)*; however, curve fitting of the real surfaces' characteristics resulted in unrealistic fractal parameters, and hence that model was abandoned. There are also various elastic–plastic contact models, but the current study is concentrated on elastic contact only. Future work may focus on elastic–plastic contact.

## RESULTS

### Effects of Mesh Densities

In this section, the effect of the mesh density of the surface profile on the different model predictions is investigated. For this purpose a polished surface is investigated (see Fig. 2). Although this surface is very smooth, there are still some noticeable scratches on the surface. In addition, one can see that the sur-

Table 1—The Variation of Surface Parameters with Scale for Surface 1

| Parameter | $1,001 \times 1,001$ | $100 \times 100$ |
|---|---|---|
| $\sigma$ ($\mu$m) | 0.4057 | 0.3925 |
| $R$ ($\mu$m) | 4.816 | 466.6 |
| $\eta$ ($10^9$/m$^2$) | 20.38 | 0.2106 |
| $m_0$ ($10^{-12}$ m$^2$) | 0.9808 | 0.1541 |
| $m_2$ | 0.0715 | 0.0002951 |
| $m_4$ ($10^{12}$ m$^{-2}$) | 0.04944 | 0.000002029 |
| $B_{max}$ | 0.0293 | 0.0031 |

face is not perfectly flat, which would be true of most surfaces in practical applications. Other than that, there do not appear to be any noticeable patterns, structures, or irregularities on the surface. There is roughness, but it appears to be at a very small scale because the surface is polished so finely. The profile of the surface is measured using a Taicaan laser profilometer with a vertical resolution of 10 nm. The measurement is made over a 1 mm × 1 mm rectangular area with a lateral resolution of $1,001 \times 1,001$ nodes (i.e., 1 $\mu$m mesh resolution). The same data are used for the 100 × 100 mesh, except that every tenth data point is used to provide a courser mesh (i.e., 10 $\mu$m mesh resolution). The statistical and other surface parameters needed to predict the real area of contact for each of the models are given in Table 1 for each mesh. The applied force was not controlled when solving the problem (i.e., it was an output of the model); however, the range of contact areas for all three surfaces is approximately the same ($10^{-3} < A_r/A_n < 10^{-1}$). This is a range typical for contact between surfaces.

The results of the models for a 100 × 100 mesh are shown in Figs. 3 and 4, and for a $1,001 \times 1,001$ mesh the results are shown in Figs. 5 and 6. The resulting trends of all the models for the two mesh densities are very similar; however, quantitatively the predictions are quite different (see Figs. 3 and 5). Most of the models using either surface mesh appear to predict a nearly linear relationship between contact area and load (see Figs. 3 and 5) and thus a nearly constant real contact pressure (see Figs. 4 and 6). When the pressure is shown as in Figs. 4 and 6, the quantitative differences are most noticeable. In addition, the deterministic and GW model (Greenwood and Williamson (2)) appear to predict a real contact pressure that is not exactly constant, and therefore the relationship between load and contact area for these models may not be linear. The models using the 100 × 100 mesh predict a real contact pressure of about 0.01·E, whereas the models using the $1,001 \times 1,001$ mesh predict about 0.1·E. The overall
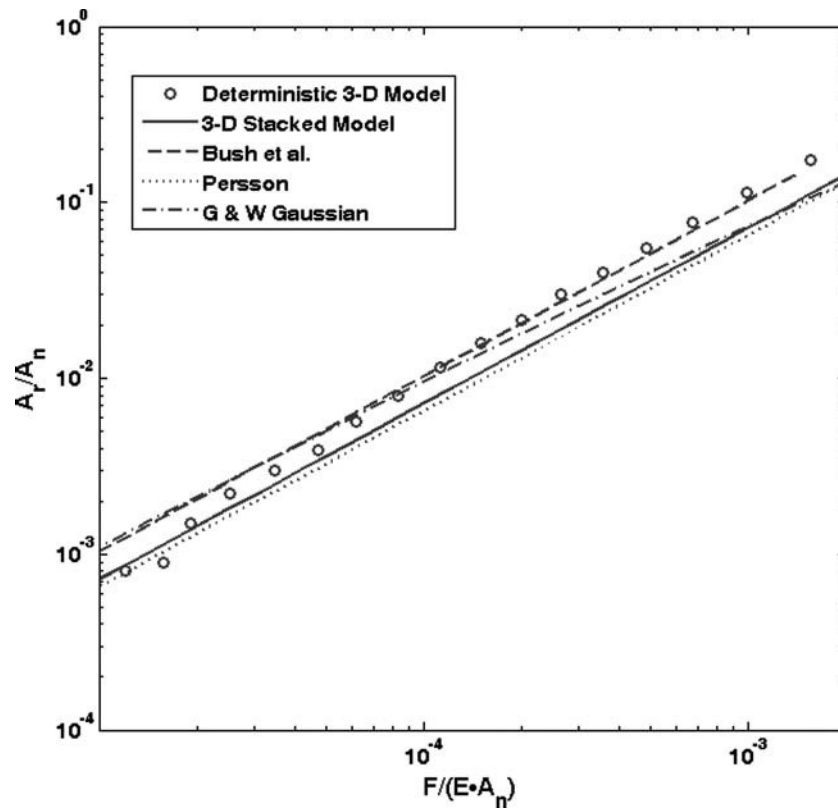
**Fig. 3—Resulting model predictions of normalized real contact area versus normalized load for a 100 × 100 course mesh of surface 1.**
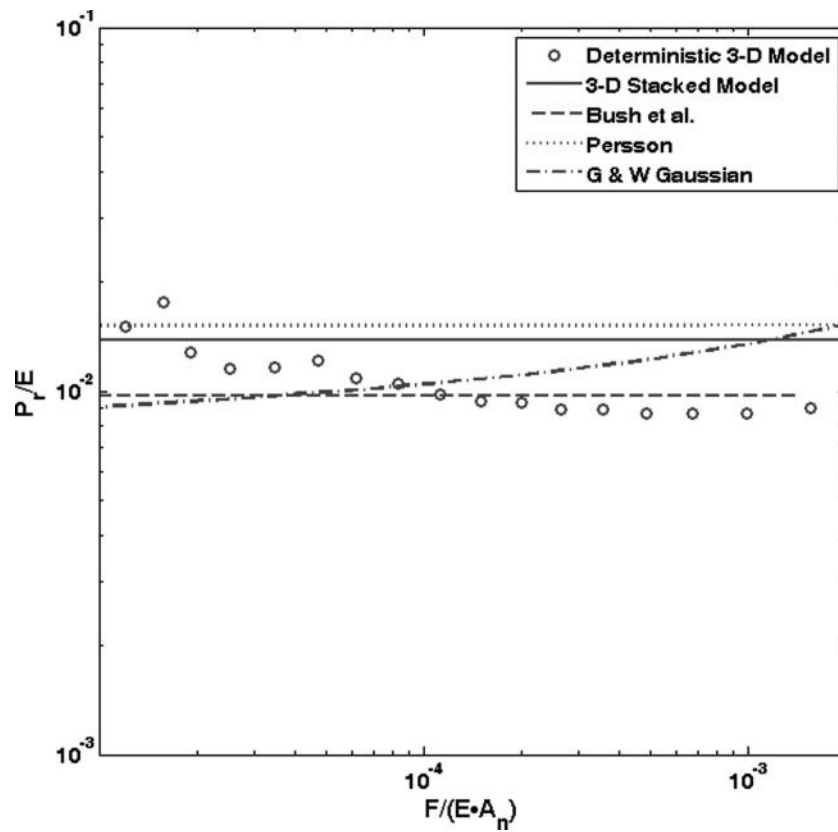


**Fig. 4—Resulting model predictions of normalized real contact pressure versus normalized load for a 100 × 100 course mesh of surface 1.**
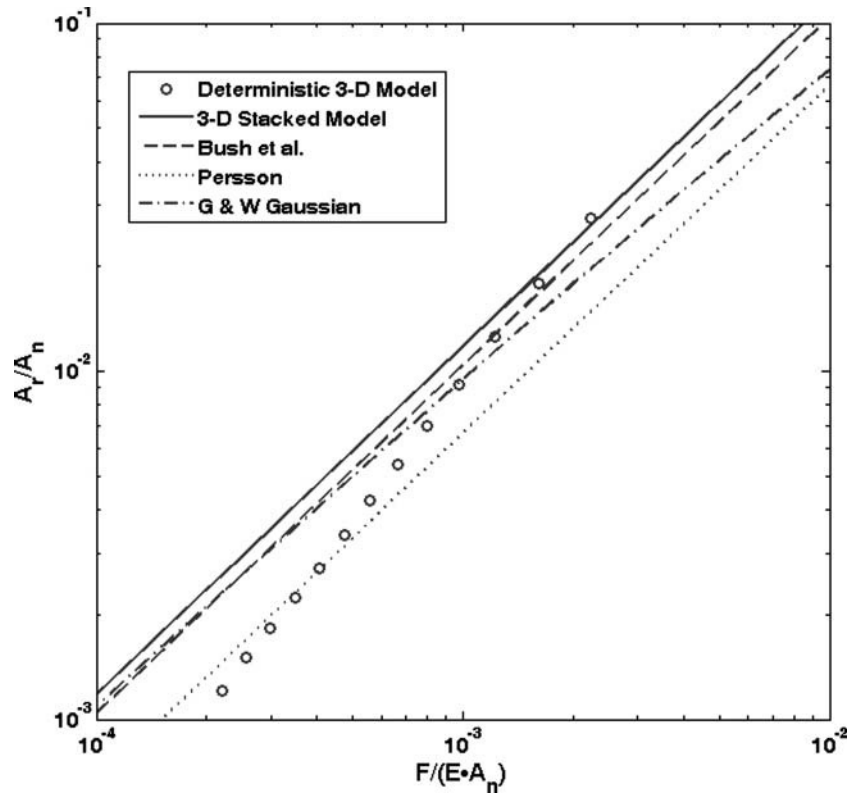
**Fig. 5—Resulting model predictions of normalized real contact area versus normalized load for a 1,001 × 1,001 fine mesh of surface 1.**
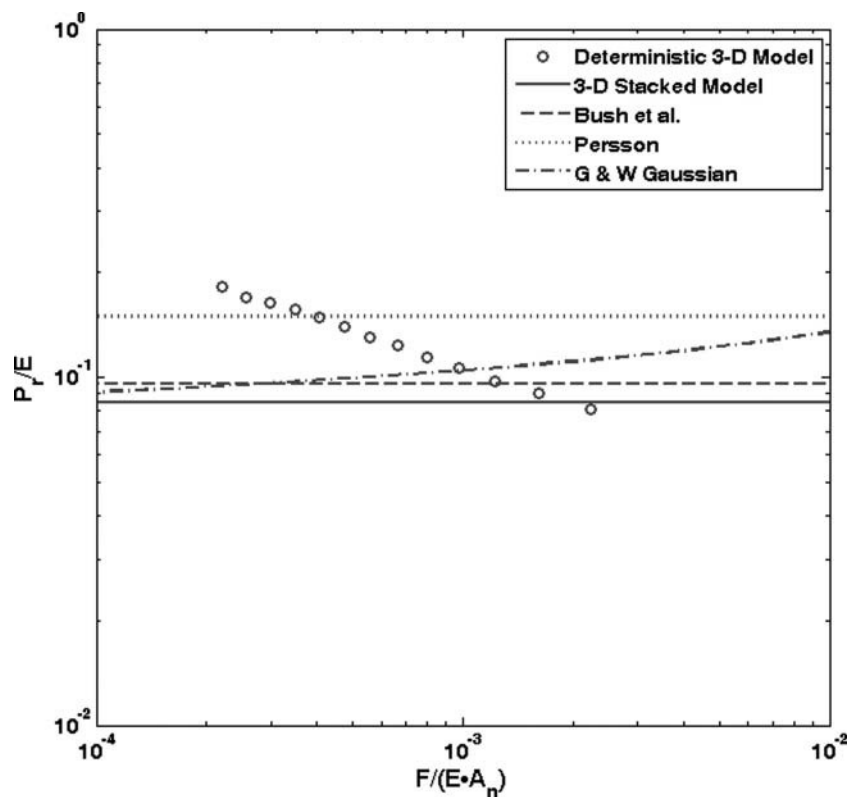


**Fig. 6—Resulting model predictions of normalized real contact pressure versus normalized load for a 1,001 × 1,001 fine mesh of surface 1.**

Table 2—Statistical and Other Parameters for Three Surfaces Using a Mesh of 1,001 × 1,001

| Parameter | Surface 1 | Surface 2 | Surface 3 |
|---|---|---|---|
| $\sigma$ ($\mu$m) | 0.4057 | 2.397 | 15.01 |
| $R$ ($\mu$m) | 4.816 | 0.6513 | 0.3558 |
| $\eta$ ($10^9$/m$^2$) | 20.38 | 20.59 | 9.088 |
| $m_0$ ($10^{-12}$ m$^2$) | 0.9808 | 0.4242 | 225.3 |
| $m_2$ | 0.0715 | 0.1143 | 12.016 |
| $m_4$ ($10^{12}$ m$^{-2}$) | 0.04944 | 0.07683 | 3.560 |
| $B_{max}$ | 0.0293 | 0.03970 | 0.1958 |

agreement between the analytical models and the deterministic model also appears to be better for the 100 × 100 mesh than for the 1,001 × 1,001 mesh. Actually, the model by Bush, et al. *(15)* appears to agree best with the 100 × 100 mesh results, especially at high loads.

### Parameters of Three Different Surfaces

Next, the predictions of the various models will be compared to each other and to the deterministic model for three different surface profiles of various roughnesses and morphologies using a lateral mesh of 1,001 × 1,001 nodes. Surfaces with very different finishes are selected in order to observe the effect that these geometrical differences have on agreement between the models. All statistical and other geometrical quantities are listed in Table 2. This includes surface 1, which was discussed in relation to the mesh density. For all the cases the effective elastic modulus, $E'$, is set to 100 GPa. Because the results are normalized and all of the models are dependent on $E'$ in the same way, the variation of $E'$ does not affect the results.

### Surface 1 Results

Surface 1, which was discussed above (see Figs. 5 and 6), is more closely examined. All the analytical model predictions are in fairly good qualitative agreement, where for higher loads the deterministic model also appears to come into good quantitative agreement with the analytical models. The deterministic model becomes more accurate when more nodes are in contact, because the stress is more evenly distributed across more asperities (nodes) and the stress gradient across them is smaller. If the average contact pressure is plotted versus the normalized force, this trend is apparent (see Fig. 6). For surface 1 it appears that the deterministic model predictions actually cross from Persson's *(12)* theory to the 3D stacked model and over all the other models in between.

### Surface 2 Results

In this section, the predictions of all the models for surface 2 are compared. The 3D profile measured for surface 2 is shown in Fig. 7. The surface has some periodic structure that is not present in surface 1. This surface is machined but not polished. There are also some noticeable scratches or wear scars on the surface that run mostly perpendicular to the periodic structure. Not only is surface 2 rougher than surface 1 but its structure also appears to be significantly different. This will also be the case when it is compared later to surface 3.

The model predictions using surface 2 show some very interesting trends (see Figs. 8 and 9). It appears that the deterministic model agrees first with the G &W Gaussian model solution and then with higher load shifts to agree better with the other models. This may be because at low loads the GW model (Greenwood and Williamson *(2)*) might be better at modeling a few
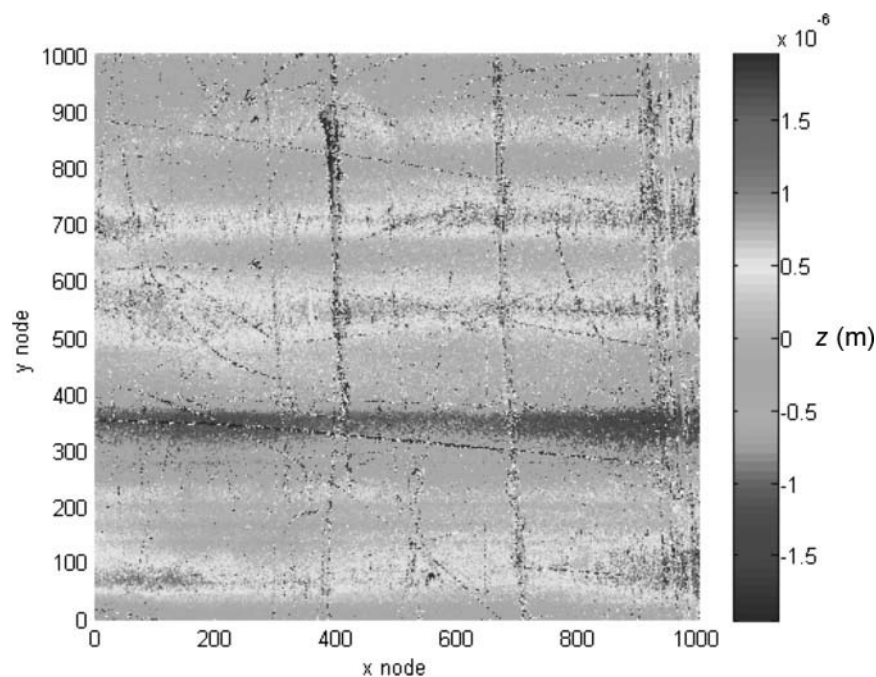

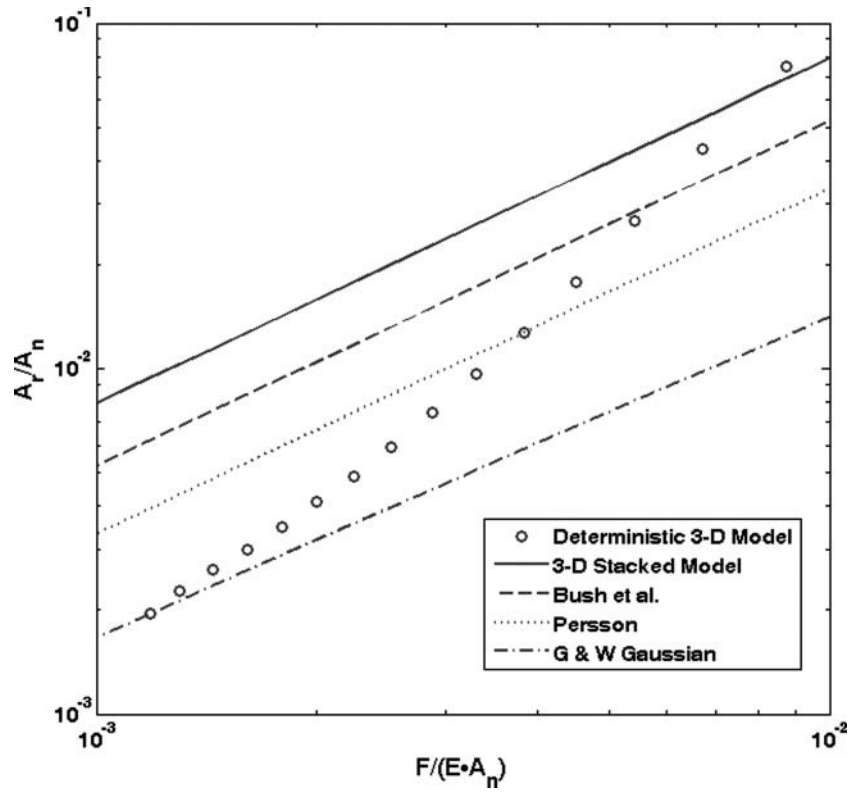
Fig. 7—Measured profile of surface 2.

**Fig. 8—Resulting model predictions of normalized real contact area versus normalized load for a 1,001 × 1,001 course mesh of surface 2.**
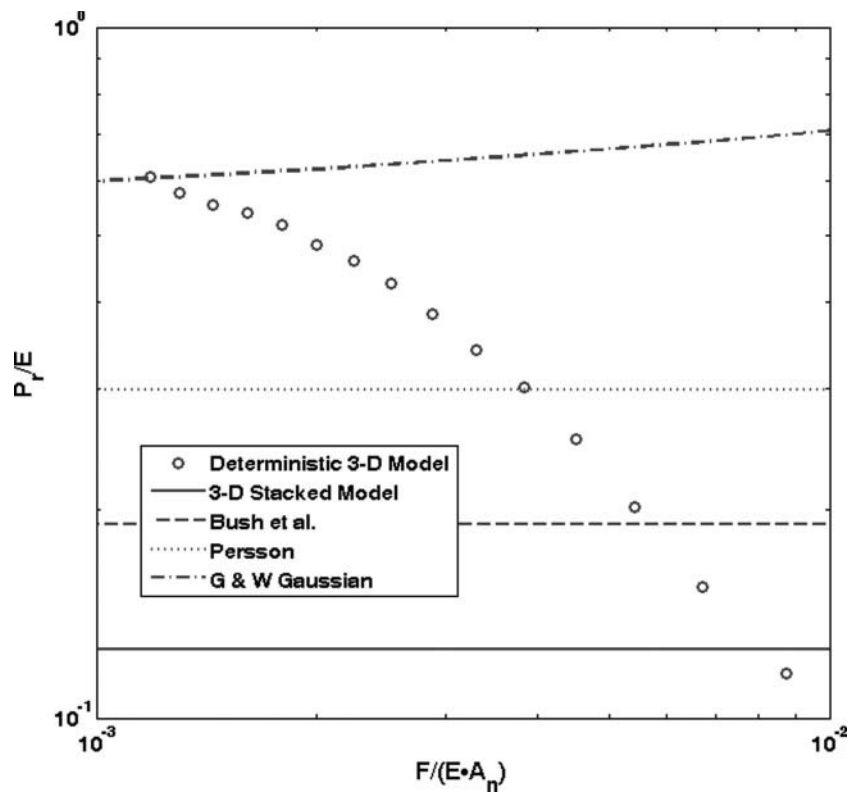


**Fig. 9—Resulting model predictions of normalized real contact pressure versus normalized load for a 1,001 × 1,001 course mesh of surface 2.**
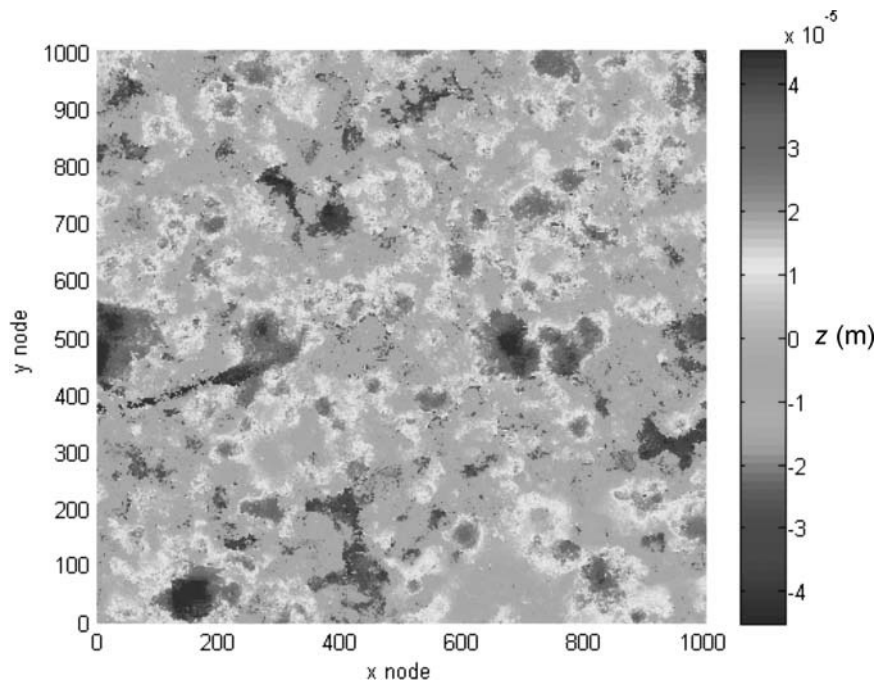
**Fig. 10—Measured profile of surface 3.**

isolated asperity contacts. Likewise, at higher loads and up to complete contact, the 3D stacked model (Jackson *(20)*) and Persson's *(12)* model are supposed to give very accurate predictions. The FFT deterministic model (Stanley and Kato *(13)*) predictions must therefore be nonlinear to transverse between the different linear models. This would also suggest that real surfaces might not always produce linear relationships between the real contact area and load. These results are also similar to those predicted by the models using data for surface 1 because for that surface the average pressure predicted by the deterministic model also decreases with load and crosses over the predictions of several different models.
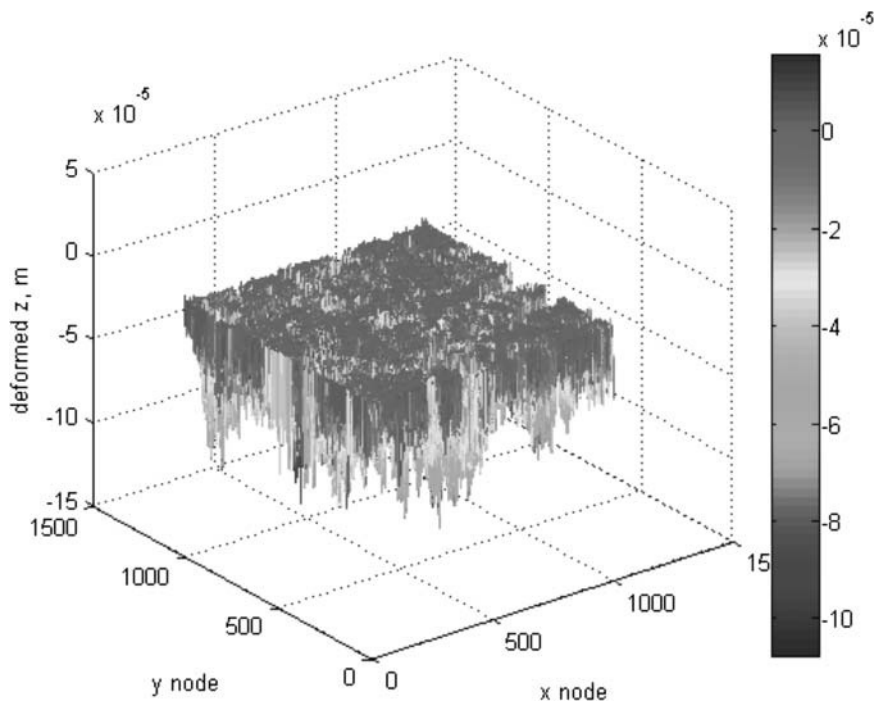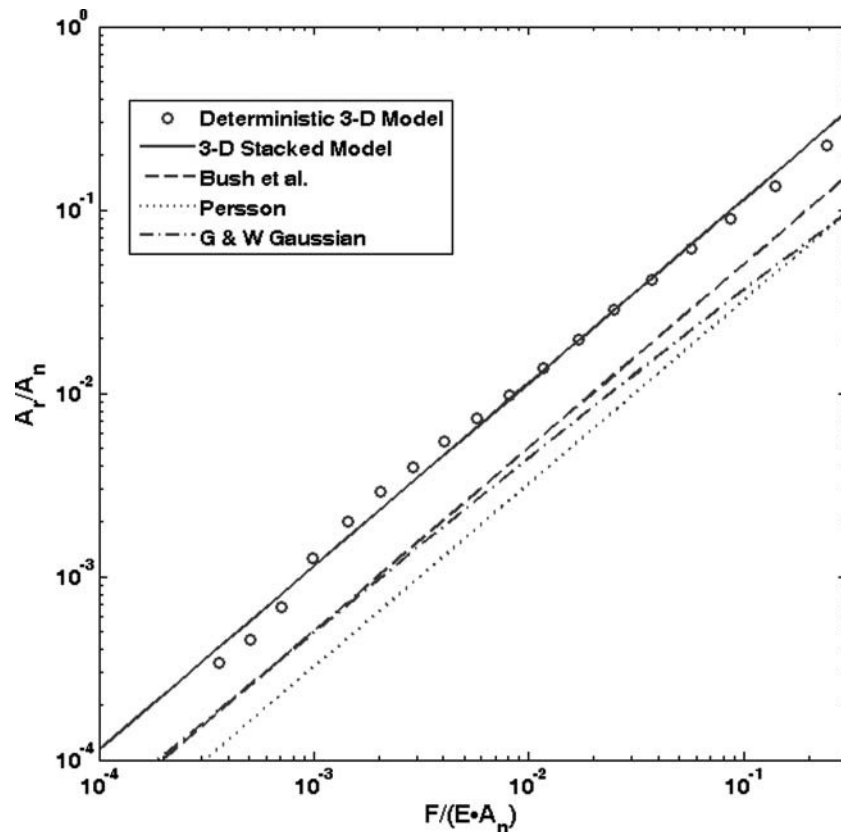


**Fig. 11—Surface 3 1,001 × 1,001 deformed profile.**

**Fig. 12—Resulting model predictions of normalized real contact area versus normalized load for a 1,001 × 1,001 course mesh of surface 3.**

## Surface 3 Results

The final surface analyzed in the current work is also the roughest and is labeled as surface 3, and likewise the predictions of all models are compared. The measured profile of surface 3 is shown in Fig. 10. The roughness of surface 3 is more isotropic than surfaces 1 and 2. There also appear to be fewer wear scars or grooves on surface 3. Because of the apparent isotropic surface structure, visually the asperities on the surface appear to be somewhat spherical (which is a common assumption used in several of the analytical models). Again, the roughness and surface structure of surface 3 is much different than both surfaces 1 and 2.

A sample view of surface 3 after being loaded and deformed by the opposing flat surface as calculated by the FFT deterministic model is shown in Fig. 11. The flattened part of the asperities is clearly shown because there are no asperities over the height of the flat surface.

The predictions of the various contact models for surface 3 are shown in Figs. 12 and 13. As with the predictions of contact area as a function of load for surfaces 1 and 2, there appears to be a nominally linear relationship between the real contact area and load for surface 3 (see Fig. 12). For this surface it appears that the stacked multiscale model (Jackson *(20)*) shows the best agreement with the deterministic model predictions, which might be surprising because it assumes that all asperities are sinusoidal in shape. The Bush, et al. *(15)* model appears to show the next best agreement, and the remaining closed-form models, includ-

ing the GW model (Greenwood and Williamson *(2)*), appear to be in relatively close agreement. It is uncertain why the stacked model is in fairly good agreement with the deterministic results for surface 3 but not as well with surfaces 1 and 2. From the plot of the real contact pressure versus load shown in Fig. 13, it is clear that all the closed-form models are within an order of magnitude of agreeing with the deterministic model.

Although all the models appear to generate the same general trends and also make predictions that differ by less than an order of magnitude, from an engineering perspective these differences are still large. The reality of rough surface contact modeling is that any surface model that reduces the surface geometry down to a few key parameters will result in merely an approximate prediction of the relationship between real contact area and contact force. Real surfaces are complex and do not precisely follow any mathematical structure (fractal, Gaussian, etc.). This results in deviations of the actual surface contact from the predictions made by the models. Therefore, one might think that deterministic models provide the best alternative. However, due to limitations of computational resources and therefore mesh densities, it is likely that the deterministic models may have limitations. Even if an adequate mesh is obtained, the deterministic model may take larger amounts of CPU time to reach a solution. This is especially impractical if the predictions are being incorporated into a larger and more extensive simulation. In addition, there can be errors in the surface measurements from stylus tip geometry,
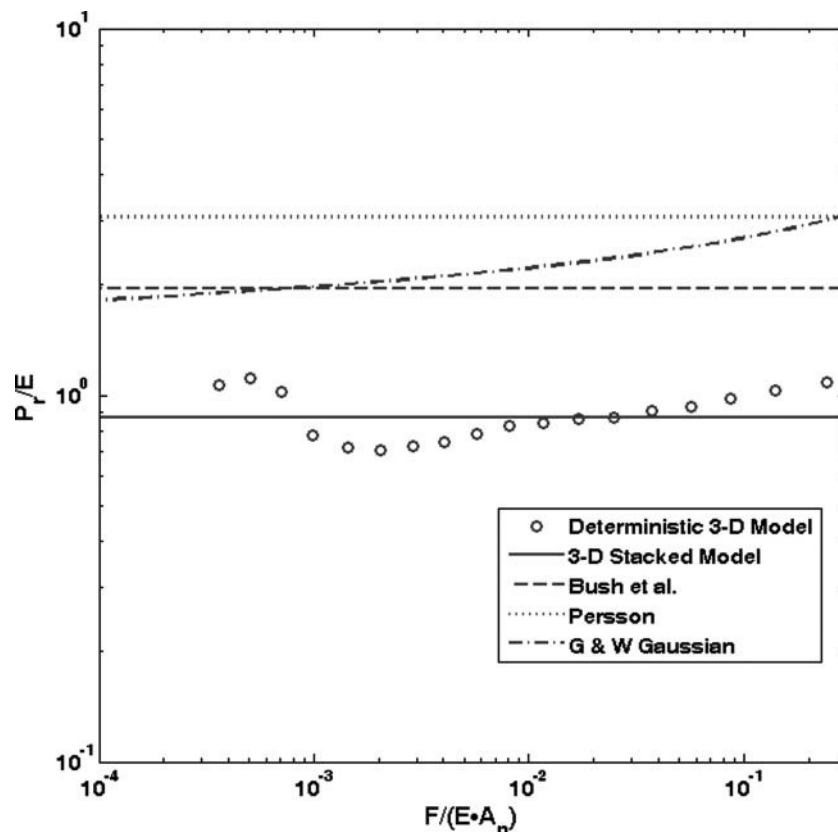
**Fig. 13—Resulting model predictions of normalized real contact pressure versus normalized load for a 1,001 × 1,001 course mesh of surface 3.**

instrument vibration, etc., that may result in errors in the deterministic model predictions.

## CONCLUSIONS

This work presents an FFT-based deterministic model of elastic contact between rough surfaces, a new closed-form solution to the Greenwood and Williamson *(2)* model, and a comparison of several closed-form elastic rough surface contact models to the deterministic models. The deterministic model is based on Stanley and Kato's *(13)* FFT deterministic elastic contact model. The other analytical models included in the comparison are the new closed-form solutions to the GW model (Greenwood and Williamson *(2)*, with a full Gaussian distribution), the Bush, et al. *(15)* statistical contact model, Persson's *(12)* diffusion contact model, and a stacked multiscale model (Jackson *(20)*).

First the effect of mesh resolution is studied for one surface by skipping points of data on the surface. The two surfaces then had a two orders of magnitude difference in the number of data points (meshes of 100 × 100 and 1,001 × 1,001). It is found that all the models are similarly affected by the scale of data that is used. Specifically, all the models using the finer mesh (1,001 × 1,001) predicted an average contact pressure approximately one order of magnitude larger than when using the course mesh (100 × 100). This also results in the models predicting a smaller contact area when the finer mesh is used.

The results for three very different surfaces show that all of the remaining models produce nearly linear predictions of contact area as a function of load and in some cases are even in quantitative agreement. This is reassuring because many of these models are based on very different mathematical foundations and assumptions. It should be noted that because most of these closed-form models reduce the complex surface profile to only a few key parameters, they cannot be expected to make exact quantitative predictions of rough surface contact. However, they all appear to be within an order of magnitude and for some cases are even closer. An alternative definition to the plasticity index that is based on a multiscale approach is discussed and presented in the Appendix.

## REFERENCES

*(1)* Archard, J. F. (1957), "Elastic Deformation and the Laws of Friction," *Proceedings of the Royal Society of London A*, **243**, pp 190-205.
*(2)* Greenwood, J. A. and Williamson, J. B. P. (1966), "Contact of Nominally Flat Surfaces," *Proceedings of the Royal Society of London A*, **295**, pp 300-319.

*(3)* Majumdar, A. and Bhushan, B. (1991), "Fractal Model of Elastic–Plastic Contact between Rough Surfaces." *Journal of Tribology*, **113**(1), pp 1-11.

*(4)* Majumdar, A. and Bhushan, B. (1990), "Role of Fractal Geometry in Roughness Characterization and Contact Mechanics of Surfaces," *Journal of Tribology*, **112**(2), pp 205-216.

*(5)* Warren, T. L. and Krajcinovic, D. (1995), "Fractal Models of Elastic–Perfectly Plastic Contact of Rough Surfaces Based on the Cantor Set," *International Journal of Solids and Structures*, **32**(19), pp 2907-2922.

*(6)* Willner, K. (2004), "Elasto-Plastic Normal Contact of Three-Dimensional Fractal Surfaces Using Halfspace Theory," *Journal of Tribology*, **126**(1), pp 28-33.

*(7)* Yan, W. and Komvopoulos, K. (1998), "Contact Analysis of Elastic–Plastic Fractal Surfaces," *Journal of Applied Physics*, **84**(7), pp 3617-3624.

*(8)* Ciavarella, M. and Demelio, G. (2001), "Elastic Multiscale Contact of Rough Surfaces: Archard's Model Revisited and Comparisons with Modern Fractal Models," *Journal of Applied Mechanics*, **68**(3), pp 496-498.

*(9)* Ciavarella, M., Murolo, G., Demelio, G., and Barber, J. R. (2004), "Elastic Contact Stiffness and Contact Resistance for the Weierstrass Profile," *Journal of the Mechanics and Physics of Solids*, **52**(6), pp 1247-1265.

*(10)* Bora, C. K., Flater, E. E., Street, M. D., Redmond, J. M., Starr, M. J., Carpick, R. W., and Plesha, M. E. (2005), "Multiscale Roughness and Modeling of MEMS Interfaces," *Tribology Letters*, **19**(1), pp 37-48.

*(11)* Jackson, R. L. and Streator, J. L. (2006), "A Multiscale Model for Contact between Rough Surfaces," *Wear*, **261**(11-12), pp 1337-1347.

*(12)* Persson, B. N. J. (2001), "Elastoplastic Contact between Randomly Rough Surfaces," *Physical Review Letters*, **87**(11), p 116101.

*(13)* Stanley, H. M. and Kato, T. (1997), "FFT-Based Method for Rough Surface Contact," *Journal of Tribology*, **119**(3), pp 481-485.

*(14)* McCool, J. I. (1986), "Comparison of Models for the Contact of Rough Surfaces," *Wear*, **107**(1), pp 37-60.

*(15)* Bush, A. W., Gibson, R. D., and Thomas, T. R. (1975), "The Elastic Contact of Rough Surfaces," *Wear*, **35**, pp 87-111.

*(16)* Persson, B. N. J., Bucher, F., and Chiaia, B. (2002), "Elastic Contact between Randomly Rough Surfaces: Comparison of Theory with Numerical Results," *Physical Review B*, **65**, p 184106-1.

*(17)* Jackson, R. L. and Green, I. (2006), "A Statistical Model of Elasto-Plastic Asperity Contact between Rough Surfaces," *Tribology International*, **39**(9), pp 906-914.

*(18)* Kogut, L. and Jackson, R. L. (2005), "A Comparison of Contact Modeling Utilizing Statistical and Fractal Approaches," *Journal of Tribology*, **128**(1), pp 213-217.

*(19)* Hyun, S., Pel, L., Molinari, J. F., and Robbins, M. O. (2004), "Finite-Element Analysis of Contact between Elastic Self-Affine Surfaces," *Physical Review E*, **70**(22), pp 026117-1-026117-12.

*(20)* Jackson, R. L. (2010), "An Analytical Solution to an Archard-Type Fractal Rough Surface Contact Model," *Tribology Transactions*, **53**(4), pp 543-553.

*(21)* Johnson, K. L., Greenwood, J. A., and Higginson, J. G. (1985), "The Contact of Elastic Regular Wavy Surfaces," *International Journal of Mechanical Sciences*, **27**(6), pp 383-396.

*(22)* Krithivasan, V. and Jackson, R. L. (2007), "An Analysis of Three-Dimensional Elasto-Plastic Sinusoidal Contact," *Tribology Letters*, **27**(1), pp 31-43.

*(23)* Etsion, I. and Front, I. (1994), "Model for Static Sealing Performances of End Face Seals," *Tribology Transactions*, **37**(1), pp 111-119.

*(24)* Polycarpou, A. and Etsion, I. (1999), "Analytical Approximations in Modeling Contacting Rough Surfaces," *Journal of Tribology*, **121**(2), pp 234-239.

*(25)* Hess, D. P. and Soom, A. (1993), "Effects of Relative Angular Motions on Friction at Rough Planar Contacts," *Journal of Tribology*, **115**(3), pp 96-101.

*(26)* Hess, D. P. and Soom, A. (1992), "Normal and Angular Motions at Rough Planar Contacts during Sliding with Friction," *Journal of Tribology*, **114**(3), pp 567-578.

*(27)* Liu, Z., Neville, A., and Reuben, R. L. (2000), "Analytical Solution for Elastic and Elastic–Plastic Contact Models," *Tribology Transactions*, **43**(4), pp 627-634.

*(28)* Chang, W. R., Etsion, I., and Bogy, D. B. (1987), "An Elastic–Plastic Model for the Contact of Rough Surfaces," *Journal of Tribology*, **109**(2), pp 257-263.

*(29)* Green, I. (2002), "A Transient Dynamic Analysis of Mechanical Seals Including Asperity Contact and Face Deformation," *Tribology Transactions*, **45**(3), pp 284-293.

*(30)* McCool, J. I. (1987), "Relating Profile Instrument Measurements to the Functional Performance of Rough Surfaces," *Journal Tribology*, **109**(2), pp 264-270.

*(31)* Jackson, R. L. (2006), "The Effect of Scale Dependant Hardness on Elasto-Plastic Asperity Contact between Rough Surfaces," *Tribology Transactions*, **49**(2), pp 135-150.

*(32)* Onions, R. A. and Archard, J. F. (1973), "The Contact of Surfaces Having a Random Structure," *Journal of Physics D: Applied Physics*, **6**, pp 289-304.

*(33)* Greenwood, J. A. (2006), "A Simplified Elliptical Model of Rough Surface Contact," *Wear*, **261**(2), pp 191-200.

*(34)* Carbone, G. and Bottiglione, F. (2008), "Asperity Contact Theories: Do They Predict Linearity Between Contact Area and Load?" *Journal of the Mechanics and Physics of Solids*, **56**(8), pp 2555-2572.

*(35)* Pei, L., Hyun, S., Molinari, J. F., and Robbins, M. O. (2005), "Finite Element Modeling of Elasto-Plastic Contact between Rough Surfaces," *Journal of the Mechanics and Physics of Solids*, **53**(11), pp 2385-2409.

*(36)* Ciavarella, M., Demelio, G., Barber, J. R., and Jang, Y. H. (2000), "Linear Elastic Contact of the Weierstrass Profile," *Proceedings of the Royal Society of London A*, **456**, pp 387-405.

*(37)* Wilson, W. E., Angadi, S. V., and Jackson, R. L. (2010), "Surface Separation and Contact Resistance Considering Sinusoidal Elastic–Plastic Multi-Scale Rough Surface Contact," *Wear*, **268**(1-2), pp 190-201.

*(38)* Kogut, L. and Etsion, I. (2003), "A Finite Element Based Elastic–Plastic Model for the Contact of Rough Surfaces," *Tribology Transactions*, **46**(3), pp 383-390.

*(39)* Jackson, R. L. and Green, I. (2005), "A Finite Element Study of Elasto-Plastic Hemispherical Contact," *Journal of Tribology*, **127**(2), pp 343-354.

*(40)* Green, I. (2005), "Poisson Ratio Effects and Critical Values in Spherical and Cylindrical Hertzian Contacts," *International Journal of Applied Mechanics and Engineering*, **10**(3), pp 451-462.

*(41)* Jackson, R. L., Krithivasan, V., and Wilson, W. E. (2008), "The Pressure to Cause Complete Contact between Elastic Plastic Sinusoidal Surfaces," *Proceedings of the Institution of Mechanical Engineerings - Part J: Journal of Engineering Tribology*, **222**(7), pp 857-864.

*(42)* Whitehouse, D. J. and Archard, J. F. (1970), "The Properties of Random Surfaces of Significance in Their Contact," *Proceedings of the Royal Society of London A*, **316**, pp 97-121.

## APPENDIX

Greenwood and Williamson *(2)* define a plasticity index from the surface properties and the critical interference, which is given in a slightly different format by Kogut and Etsion *(38)* as:

$$\Psi = \sqrt{\frac{\sigma_s}{\omega_c}} \qquad [A1]$$

The critical interference to cause plastic deformation for a spherical Hertz contact is given by Jackson and Green *(39)* as:

$$\omega_c = \left(\frac{\pi \cdot (CS_y)}{2E'}\right)^2 R \qquad [A2]$$

According to Green [40] the value of $CS_y = \min(C(v_1) S_{y1}, C(v_2) S_{y2})$, accounts for the possibility of contact between dissimilar materials, where $C(v) = 1.295\exp(0.736v)$. This is because the surface with the minimum $CS_y$ value will be the first to yield. Note that Eq. [A2] differs from the version offered by Chang et al. *(28)* in that it is based on the well-defined yield strength rather than on a loosely-defined hardness with a corresponding hardness factor. Substituting Eq. [A2] into Eq. [Al] results in

$$\psi = \frac{2E'}{\pi \cdot 1.295e^{0.736v} \cdot S_y} \sqrt{\frac{\sigma_s}{R}} \qquad [A3]$$

The plasticity index relates the critical interference and the roughness of the surface to the plastic deformation of the surface. According to Greenwood and Williamson *(2)*, the critical value of the plasticity index marking the boundary of predominantly elastic contact and elastic-plastic contact is approximately unity. A higher plasticity index indicates a surface whose asperities are

more likely to yield. Asperities are thus more likely to deform plastically on rougher surfaces with lower critical interference values. Greenwood and Williamson *(2)* suggest that for real surfaces the plasticity index can range from $\psi = 0.1$ to $\psi = 100$. Since the plasticity index is dependent on the rms roughness of the surface peaks $(\sigma_s)$ it is also dependent on the scale of the employed surface data [18]. However, from the multiscale surface contact methodology set forth by Jackson and Streator *(11)* and developed further by Wilson et al. *(37)*, an alternative plasticity index can be derived. Wilson et al. expanded the multiscale methodology by including an FEM elastic-plastic sinusoidal contact model *(22, 41)*. A critical amplitude, $\Delta_c$, is analytically derived using the von Mises yield criteria below which a sinusoidal contact ($\Delta <$ .$\Delta_c$) will deform purely elastically and is given as

$$\Delta_c = \frac{\sqrt{2}S_y e^{\frac{2}{3}\nu}}{3\pi E' f} \qquad [A4]$$

where $\Delta$ is the amplitude of the sinusoidal surface and $f$ is the frequency (the reciprocal of the wavelength, $1/\lambda$). Again, when ($\Delta < \Delta_c$, a sinusoidal surface will always deform elastically only, even to the point of complete flattening. $B$ is now defined as the ratio of the amplitude to the wavelength of a sinusoidal surface.

The critical value of $B$ can then be calculated by

$$B_c = \frac{\sqrt{2}}{3\pi} \frac{S_y}{E'} e^{\frac{2}{3}\nu} \qquad [A5]$$

Then $B_c$ can be compared to the maximum amplitude to wavelength ratio found from an FFT of a surface ($B_{max}$). If $B_{max} < B_c$, then the contact is completely elastic over all loads. Therefore an alternative plasticity index can be calculated by

$$\psi_m = \frac{B_{\max}}{B_c} = \frac{3\pi E'}{\sqrt{2}e^{2/3\nu} \cdot S_y} \left(\frac{\Delta}{\lambda}\right)_{\max} \qquad [A6]$$

Note that this does assume that the stresses of the different scales of asperities do not influence each other. Comparing Eq. [A6] and Eq. [A3], reveals clear similarities in form. It appears that there is a correlation between the geometric nondimensional parameters $\sqrt{\frac{\sigma_s}{R}}$ and $\left(\frac{\Delta}{\lambda}\right)_{\max}$. Therefore when $\psi_m$ is less than unity, Eq. [A6] predicts that the surface is deforming perfectly elastically even when the surfaces are in contact everywhere (complete contact) and deforms purely elastically for all loads. Other versions of the plasticity index are also provided in the literature that are aimed to predict the importance of plasticity using a number of different surface geometry parameters *(33, 38, 42)*.